Electronic Supplementary Material (ESI) for RSC Advances

Enhanced E → Z Photoisomerisation of 2-Aminoazobenzene

José A. Gámez, Axel Koslowski and Walter Thiel

Supporting Information

(A total of 11 pages)

Computational Details

The semiempirical OM2/MRCI approach was employed to characterise the most relevant features of the potential energy surfaces (PES) involved in this photoreaction, i. e. S_0 and S_1. The general performance of the OM2/MRCI method for excited-state properties has been assessed in comprehensive validation studies.[1-3] OM2/MRCI has been shown to provide realistic results for a variety of different photoinduced processes.[3-16] We have successfully applied this method in several recent excited-state dynamics studies, including the photoisomerisation of azobenzene (AB) and 4-aminoazobenzene (4-aAB).[2, 3, 17] Restricted open-shell Hartree-Fock (ROHF) calculations,[18] using the semiempirical OM2 Hamiltonian[19-21] with standard parameters, were performed to generate a set of initial molecular orbitals (MOs). Multi-reference configuration interaction (MRCI) calculations[22] were carried out using a (12,11) active space with 12 electrons in 11 MOs. In the ROHF solution for the planar *E*-isomer, the active MOs are the four highest doubly occupied π orbitals, the doubly occupied nitrogen lone pair of the amino group, the singly occupied nitrogen lone pair of the azo motif (HOMO in the closed-shell case), the singly occupied π orbital (LUMO in the closed-shell case), and the four lowest unoccupied π* orbitals. Like for AB and 4-aAB, three reference configurations were selected, i.e., the ROHF configuration with two singly occupied MOs and the two corresponding closed-shell determinants with doubly occupied HOMO and LUMO, respectively. The MRCI expansion comprised all single and double excitations from the reference configurations. All relevant minima were characterized by frequency analyses. Conical intersections[23] were located using a Lagrange-Newton algorithm for optimization.[24]

The time evolution of the system was modelled with non-adiabatic dynamics using Tully's surface-hopping algorithm[25, 26] with an empirical decoherence correction[27] (d=0.1 hartree). There are two possible ways to generate the set of initial conditions (structures and velocities). One procedure selects random snapshots from a classical ground-state trajectory, which is usually thermalized at 300 K (with the kinetic energy being much below the zero-point vibrational energy). Alternatively, the initial conditions can be obtained by sampling a harmonic-oscillator Wigner distribution[28] (with a much larger initial kinetic energy). It has recently been shown that sub-picosecond surface hopping dynamics yield similar results regardless of the initial sampling method.[29] In the present study, Wigner sampling was applied to generate the set of initial conditions. All molecular trajectories were started in the S_1 state. The nuclear motion was propagated using the velocity Verlet algorithm[30] with a constant time step of 0.1 fs, and between two such steps, the time-dependent electronic Schrödinger equation was propagated in intervals of 0.001 fs. The dynamics were performed on the fly, i. e. at each nuclear geometry the OM2/MRCI(12,11) energies and gradients of the two lowest singlet states were computed, and the corresponding full non-adiabatic coupling matrix elements were calculated analytically. For the *Z* → *E* reaction, a total of 984 trajectories were run and followed for a maximum of 800 fs, whereas for the *E* → *Z* inverse reaction 861 and 865 trajectories were sampled for rotamers I and II, respectively, and propagated up to a maximum of 1800 fs. Photoproducts were determined by monitoring the CNNC torsion angle after the system hops back to the ground state. The OM2/MRCI(12,11) calculations (geometry optimizations and non-adiabatic dynamics) were carried out with the MNDO code.[31] More details about the implementation of surface-hopping dynamics in the MNDO program and the default conventions can be found elsewhere.[26, 32]

Rotational Barrier of the E-isomer of 2-Aminoazobenzene (2-aAB)

Fig. S1 depicts an energy profile of the E-isomer of 2-aAB along the CCNN torsion angle. As seen in the figure, both rotamers are nearly denegerate (rotamer II is ca. 0.5 kcal mol^{-1} less stable than rotamer I) but there is an energy barrier of 5 kcal mol^{-1} for the interconversion between the two rotamers.

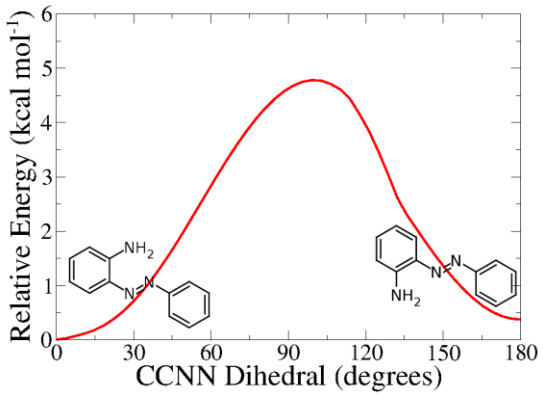

Figure S1. Energy profile of the E-isomer of 2-aAB for rotation around the C-N bond

Bonding analysis in 2-aAB

Computational Chemistry provides several bonding analysis techniques to check for the existence of hydrogen bonding in molecules. Non-Covalent Interaction (NCI)-plots show in a pictorial way where hydrogen bonds and other non-covalent interactions are located in the molecule. [33, 34] They identify regions where the reduced density gradient and the electronic density (ρ(r)) are small, which is characteristic of non-covalent interactions. By contrast, covalent interactions or bonds are found in regions where the reduced density gradient is close to zero while the electronic density is large. The sign of the second Laplacian (λ_2) of ρ(r) distinguishes between attractive or bonded ($\lambda_2 < 0$) and repulsive or nonbonded ($\lambda_2 > 0$) interactions, while the magnitude of ρ(r) estimates the strength of the interaction: the larger ρ(r), the stronger the non-covalent interactions. Fig. S2 shows the NCI-plots for the Z-isomer and for both rotamers of the E-isomer. The NCI-plots clearly indicate that I-E-2-aAB has a strong intramolecular hydrogen bond (blue regions on the left hand side of the figure) that is not present in rotamer II or the Z-isomer, where the N-H···N interactions are much weaker (green regions).

This picture is confirmed by a *Quantum Theory of Atoms-in-Molecules* (QTAIM) analysis,[35, 36] which identifies bonding interactions by first-order saddle-points of the electronic density, the so-called bond critical points (bcp). For the N-H···N interaction, no bcp could be located in rotamer II of E-2-aAB. The bcp found for E-I-2-aAB has a much higher electron density (0.03113 e a_0^{-3}) than that for Z-2-aAB (0.01098 e a_0^{-3}). The bond strength has an exponential relation with the electron density at the bcp,[36] so the QTAIM analysis again suggests a strong hydrogen bond in rotamer I of E-2-aAB that is absent in the other 2-aAB

species.

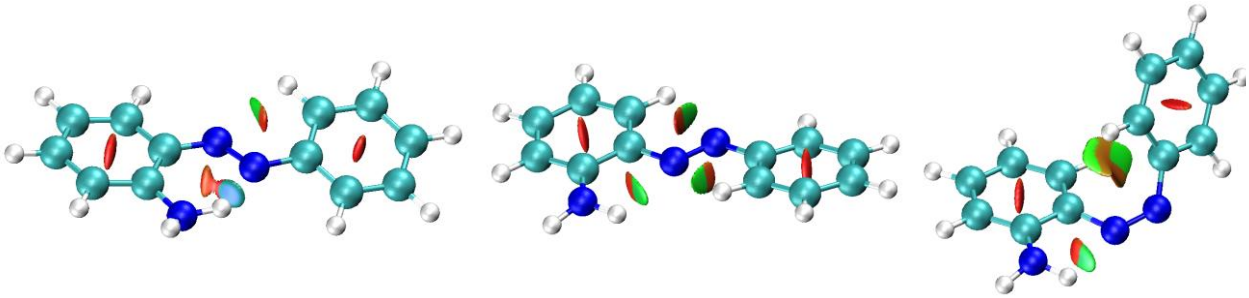

I-E-2-aAB II-E-2-aAB Z-2-aAB

Figure S2. NCI-plots for rotamer I (left) and II (middle) of the E-isomer and for the Z-isomer (right) of 2-aAB. Colour code: red, regions with strongly repulsive non-covalent interactions (e.g. steric repulsion); brown, with weakly repulsive non-covalent interactions; green, with weakly attractive non-covalent interactions (e.g. van der Waals interactions); and blue, with strongly attractive non-covalent interactions (e.g. hydrogen bonds)

Finally, Natural Bonding Orbital (NBO) analysis can be applied to assess the strength of hydrogen bonding.[37, 38] NBOs are localised orbitals, which correspond to chemical bonds when they are localised between two atoms, or to lone pairs or core pairs where they are centred on one atom. Within this framework, the strength of the hydrogen bond in 2-aAB can be estimated by the stabilisation energy produced when the lone-pair of the azo nitrogen atom is allowed to delocalise into the amino σ*(N-H) antibonding orbital. These energies are 7.86, 0.85, and 1.06 kcal mol^{-1} for rotamers I and II of E-2-aAB and for Z-2-aAB, respectively. Again, rotamer I of E-2-aAB shows a much stronger hydrogen bond than the other two species.

Geometries of the minimum-energy conical intersections (MECIs)

Table S1. Cartesian coordinates (in Å) of the four MECIs with *M*-helical chirality. Those with *P*-helical chirality are the corresponding mirror images.

	I			II			III			IV		
C	0.0000	0.0000	0.0000	0.0000	0.0000	0.0000	0.0000	0.0000	0.0000	0.0000	0.0000	0.0000
C	1.4314	0.0000	0.0000	1.4314	0.0000	0.0000	1.4314	0.0000	0.0000	1.4314	0.0000	0.0000
C	2.1495	1.2141	0.0000	2.1495	1.2141	0.0000	2.1495	1.2141	0.0000	2.1495	1.2141	0.0000
C	1.4599	2.4177	0.0346	1.4599	2.4177	0.0346	1.4599	2.4177	0.0346	1.4599	2.4177	0.0346
C	0.0618	2.4303	0.0587	0.0618	2.4303	0.0587	0.0618	2.4303	0.0587	0.0618	2.4303	0.0587
C	-0.6642	1.2437	0.0376	-0.6642	1.2437	0.0376	-0.6642	1.2437	0.0376	-0.6642	1.2437	0.0376
N	2.1466	-1.1928	-0.0269	2.1466	-1.1928	-0.0269	2.1466	-1.1928	-0.0269	2.1466	-1.1928	-0.0269
N	1.8659	-2.3716	-0.1048	1.8659	-2.3716	-0.1048	1.8659	-2.3716	-0.1048	1.8659	-2.3716	-0.1048
C	1.7812	-3.1826	1.0837	1.7812	-3.1826	1.0837	1.7812	-3.1826	1.0837	1.7812	-3.1826	1.0837
C	1.7476	-4.5768	0.8971	1.7476	-4.5768	0.8971	1.7476	-4.5768	0.8971	1.7476	-4.5768	0.8971
C	1.6371	-5.3958	2.0157	1.6371	-5.3958	2.0157	1.6371	-5.3958	2.0157	1.6371	-5.3958	2.0157
C	1.5660	-4.8394	3.2946	1.5660	-4.8394	3.2946	1.5660	-4.8394	3.2946	1.5660	-4.8394	3.2946
C	1.6051	-3.4535	3.4698	1.6051	-3.4535	3.4698	1.6051	-3.4535	3.4698	1.6051	-3.4535	3.4698
C	1.7163	-2.6122	2.3672	1.7163	-2.6122	2.3672	1.7163	-2.6122	2.3672	1.7163	-2.6122	2.3672
N	-0.7181	-1.1716	0.0196	-0.5695	-0.9292	0.0155	-0.5695	-0.9292	0.0155	-0.5695	-0.9292	0.0155
H	3.2403	1.1789	-0.0167	3.5886	1.1676	-0.0221	3.2388	1.1789	-0.0167	3.2388	1.1789	-0.0167
H	-1.7563	1.2620	0.0542	-1.7563	1.2620	0.0542	-1.7563	1.2620	0.0542	-1.7563	1.2620	0.0542
H	2.0127	3.3610	0.0436	2.0127	3.3610	0.0436	2.0127	3.3610	0.0436	2.0127	3.3610	0.0436
H	-0.4720	3.3871	0.0859	-0.4720	3.3871	0.0859	-0.4720	3.3871	0.0859	-0.4720	3.3871	0.0859
H	1.7510	-1.5286	2.4936	1.7510	-1.5286	2.4936	1.7510	-1.5286	2.4936	1.7621	-1.1827	2.5339
H	1.8092	-4.9900	-0.1113	1.8092	-4.9900	-0.1113	1.8289	-5.1219	-0.4332	1.8092	-4.9894	-0.1099
H	1.5504	-3.0291	4.4773	1.5504	-3.0291	4.4773	1.5504	-3.0291	4.4773	1.5504	-3.0291	4.4773
H	1.6075	-6.4837	1.8912	1.6075	-6.4837	1.8912	1.6075	-6.4837	1.8912	1.6075	-6.4837	1.8912
H	1.4829	-5.4939	4.1697	1.4829	-5.4939	4.1697	1.4829	-5.4939	4.1697	1.4829	-5.4939	4.1697
H	-1.7025	-1.1264	-0.1514	3.9552	2.1066	-0.0192	1.7911	-6.1281	-0.3869	1.7042	-0.9567	3.5146
H	-0.2919	-2.0228	-0.2869	3.8966	0.6891	-0.8541	2.6965	-4.8375	-0.8604	2.6276	-0.8281	2.1580

Definition of helical chirality

Chirality in molecules arises not only from stereogenic centres such as asymmetric carbon atoms. There are also planar and axial chiral elements.[39] The chirality in Z-2-aAB and in the MECIs results from the helicity along the CCNNCC motif (atoms 1-6 in Fig. S3). To determine the rotation of the helix, the molecule is oriented with one phenyl ring in the front and the other one in the back. The movement along the helix defined by atoms 1-6 follows either a clockwise or counterclockwise rotation (left and right hand side of Fig. S3). By definition, the clockwise helix has *P* (or plus) helicity, while the counterclockwise helix has *M* (or minus) helicity. The chiral axis lies in the direction of the helix thread, perpendicular to the plane bisecting the angle between the 1-2-3 and 4-5-6 planes.

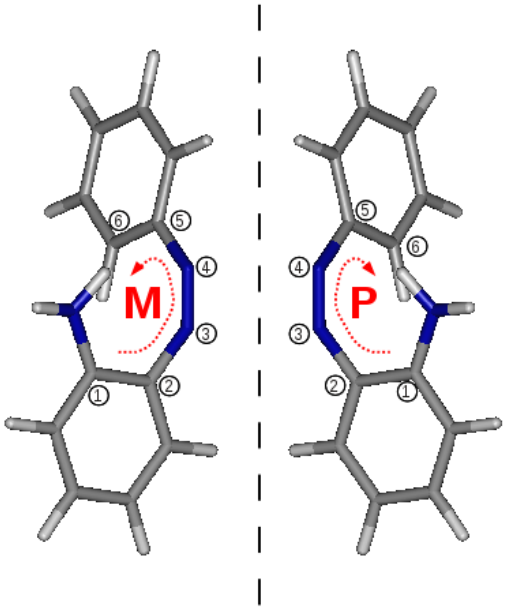

Figure S3. Helical chirality in a MECI of 2-aAB.

Distribution of CNNC dihedral angles at the hopping points

In the main manuscript, the helical chirality of the Z isomer was shown to be highly preserved during the Z → E reaction. Fig. S4 depicts energy profiles along pathways generated by linear interpolation of internal coordinates (LIIC) between the Franck Condon (FC) and MECI regions for 2-aAB (in red). There are two such pathways: one links the *M*-chiral Z-isomer with the *M*-MECI (keeping the helical chirality, solid line) while the other one connects the *M*-Z-form with the *P*-MECI (changing the helical chirality, dashed line). Obviously, the pathway keeping the helical chirality has lower energies, explaining why most trajectories arrive at the hopping point with the same helical chirality as that of the initial Z-2-aAB. More specifically, 68 % of the trajectories keep the helical chirality in 2-aAB, less so than in the case of 4-aAB (80 %) and AB (77 %). For the sake of comparison, Fig. S4 also shows the corresponding energy profiles for 4-aAB (in black). The energy difference between the enantioselective (solid line) and non-enantioselective (dashed line) pathways is larger for 4-aAB than for 2-aAB, consistent with the higher percentage of chirality-preserving trajectories in 4-aAB.

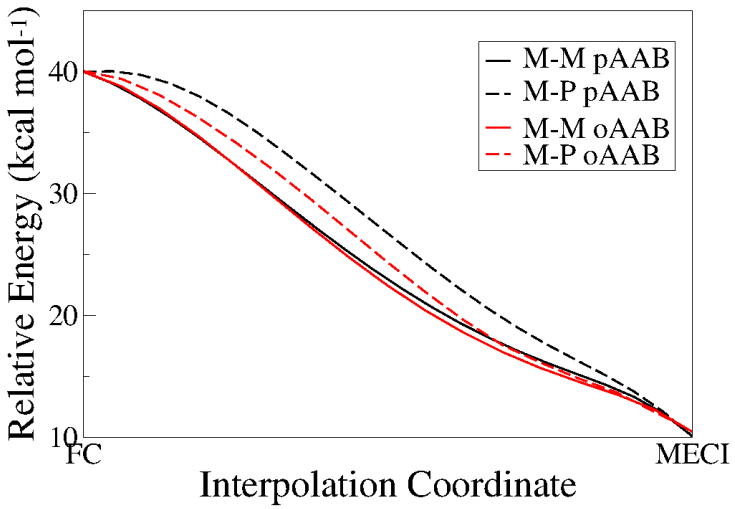

Figure S4. Energy profile along the LIIC pathways between the FC region of the Z-isomer and MECI regions for 2-aAB (oAAB, in red) and 4-aAB (pAAB, in black). Solid lines, pathways that preserve the helical chirality; dashed lines, pathways with a change in the helical chirality.

Since the E isomer is nearly planar, helical chirality should not be relevant in the reverse E → Z photoisomerisation. This is confirmed by our dynamical simulations (Fig. S5), which show that trajectories starting from the E-isomer arrive at the hopping point approximately equally distributed along the two helical-chiral channels. This is true for both rotamers I and II of E-2-aAB.

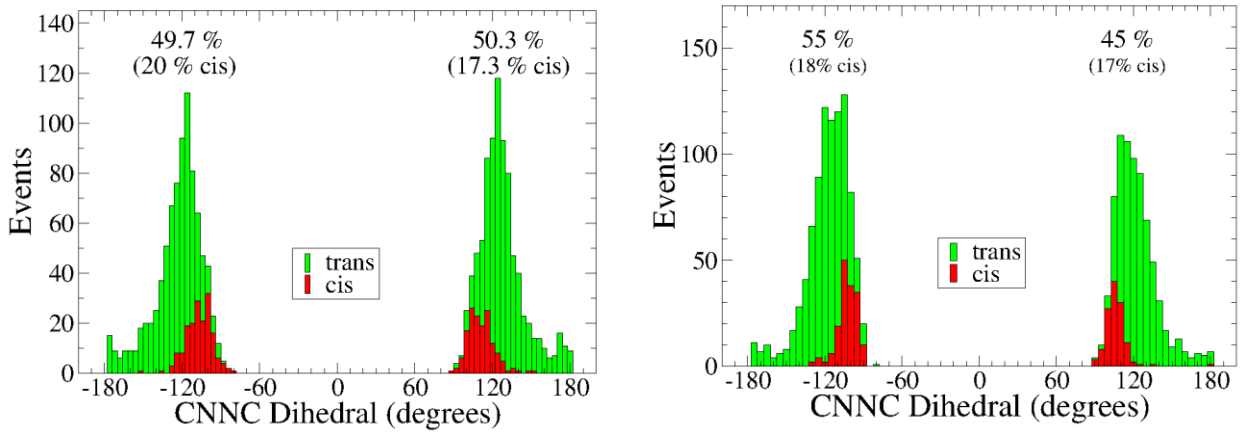

Figure S5. Distribution of CNNC dihedral angles at the hopping point for the E → Z photoisomerisation of rotamers I (left) and II (right) of E-2-aAB.

Hopping time distribution and reaction mechanism

In both the Z → E and E → Z photoisomerisation of 2-aAB, the decay to the ground state occurs in an oscillatory fashion. As shown in Fig. S6, periods with many hops to the ground state alternate with others where few or no hops are observed. Hence, the decay to the ground state is not exponential (see Fig. S7). Instead, rapid variations of the S_0 and S_1 populations alternate with plateaus with practically constant population. The time derivative of the S_0 population (blue insets in Fig. S7) reflects the oscillatory features in the time distribution of the hopping events. Indeed, the Fourier transform of the time derivative of the S_0 population gives single signals at 954, 412, and 235 cm^{-1} for Z-aAB and for rotamers I and II of E-2-aAB, respectively. As in the case of AB and 4-aAB, there are vibrational modes of the S_1 state[40] with fundamental harmonic wavenumbers that are close to the values above from Fourier analysis. In all cases, they correspond to modes involving mainly the rotation of the N_2 motif (Fig. S8). The energy gradient difference and derivative coupling vectors of the MECIs also mainly involve a rotation of the N-N bond (Fig. S9). These two vectors form the branching space of the conical intersection. They point into the directions, in which the degeneracy of the conical intersection is lifted, or in other words, where to proceed when passing from S_1 to S_0. The rotation of the N_2 motif thus plays a dominant role both in the periodic decay and the branching space. Therefore, it is evidently the rotation of the N-N bond, which is mechanistically decisive. It pulls the phenyl rings and triggers the isomerisation of the molecule. This so-called bicycle-pedal mechanism has been previously suggested[41-44] and has been confirmed in our work on AB and 4-aAB.[2, 3, 17] The existence of a common reaction mechanism for AB, 4-aAB, and 2-aAB may explain why the quantum yield of this photoreaction is not influenced much by substitution.

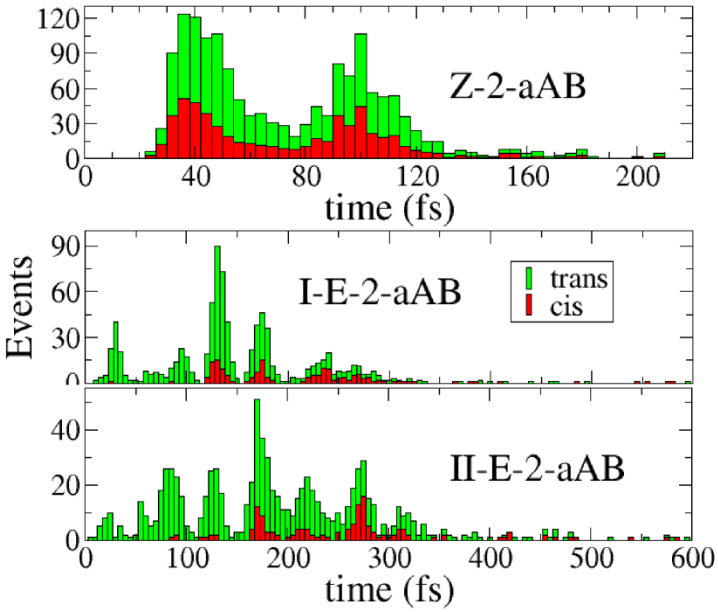

Figure S6. Distribution of hopping events with time for the Z-isomer (top) and for rotamers I (middle) and II (bottom) of the E-isomer of 2-aAB.

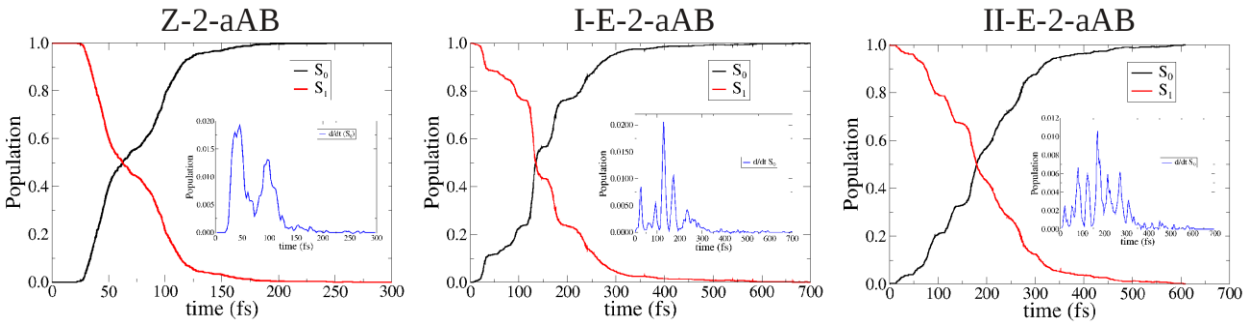

Figure S7. Population of S_0 (black) and S_1 (red) as a function of time after excitation to S_1 in Z-2-aAB (left) and in rotamers I (middle) and II (right) of E-2-aAB. The time evolution of the derivative of the S_0 population is shown in the insets (in blue).

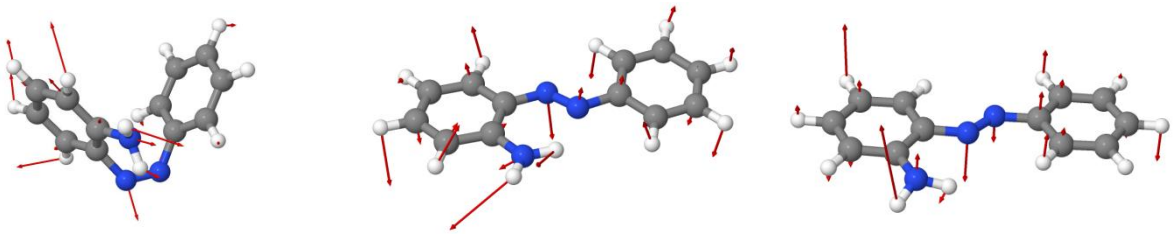

Figure S8. Vibrational modes in the ground state of Z-2-aAB at 937 cm^{-1} (left) and in the S_1 state of Z-2-aAB at 402 cm^{-1} (middle, rotamer I) and 206 cm^{-1} (right, rotamer II). The Fourier analysis of the time derivative of the S_0 population yields signals at 954, 412, and 235 cm^{-1}, respectively, which are quite close to the computed harmonic wavenumbers of the vibrations displayed above.

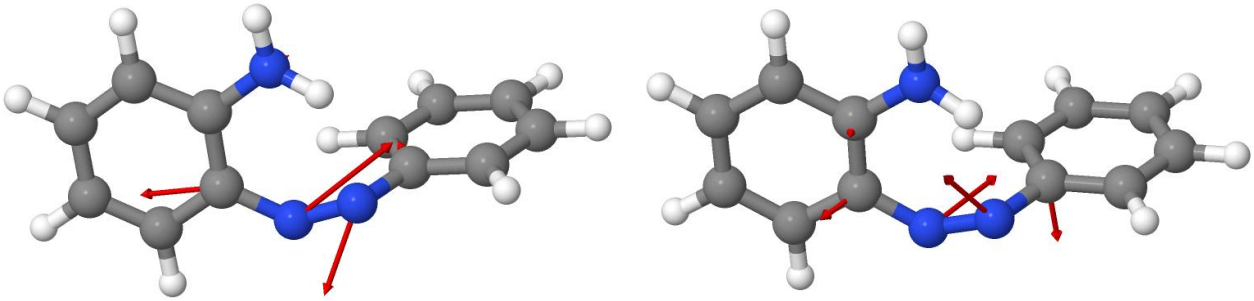

Figure S9. Vectors defining the branching space of the MECI of 2-aAB: energy gradient difference (left) and derivative coupling (right).

References

1. M. R. Silva-Junior and W. Thiel, *J. Chem. Theory Comput.*, 2010, **6**, 1546-1564.
2. J. A. Gamez, O. Weingart, A. Koslowski and W. Thiel, *J. Chem. Theory Comput.*, 2012, **8**, 2352-2358.
3. O. Weingart, Z. Lan, A. Koslowski and W. Thiel, *J. Phys. Chem. Lett.*, 2011, **2**, 1506-1509.
4. M. Hoffmann, M. Wanko, P. Strodel, P. H. König, T. Frauenheim, K. Schulten, W. Thiel, E. Tajkhorshid and M. Elstner, *J. Am. Chem. Soc.*, 2006, **128**, 10808-10818.
5. A. Kazaryan, Z. G. Lan, L. V. Schafer, W. Thiel and M. Filatov, *J. Chem. Theory Comput.*, 2011, **7**, 2189-2199.
6. K. Welke, J. S. Framcke, H. C. Watanabe, P. Hegemann and M. Elstner, *J. Phys. Chem. B*, 2011, **115**, 15119-15128.
7. G. Cui, Z. Lan and W. Thiel, *J. Am. Chem. Soc.*, 2011, **134**, 1662-1672.
8. Y. Lu, Z. Lan and W. Thiel, *Angew. Chem. Int. Ed.*, 2011, **50**, 6864-6867.
9. Z. G. Lan, Y. Lu, E. Fabiano and W. Thiel, *ChemPhysChem*, 2011, **12**, 1989-1998.
10. Z. G. Lan, E. Fabiano and W. Thiel, *ChemPhysChem*, 2009, **10**, 1225-1229.
11. E. Fabiano and W. Thiel, *J. Phys. Chem. A*, 2008, **112**, 6859-6863.
12. Z. Lan, E. Fabiano and W. Thiel, *J. Phys. Chem. B*, 2009, **113**, 3548-3555.
13. Y. Lu, Z. Lan and W. Thiel, *J. Comput. Chem.*, 2012, **33**, 1225-1235.
14. Z. Lan, Y. Lu, O. Weingart and W. Thiel, *J. Phys. Chem. A*, 2012, **116**, 1510-1518.
15. G. Cui and W. Thiel, *Phys. Chem. Chem. Phys.*, 2012, **14**, 12378-12384.
16. G. Cui and W. Thiel, *Angew. Chem., Int. Ed.*, 2013, **52**, 433-436.
17. J. A. Gamez, O. Weingart, A. Koslowski and W. Thiel, *Phys. Chem. Chem. Phys.*, 2013, **15**, 11814-11821.
18. M. J. S. Dewar, J. A. Hashmall and C. G. Venier, *J. Am. Chem. Soc.*, 1968, **90**, 1953-1957.
19. W. Weber, *Ph.D. Thesis*, University of Zürich, 1996.
20. W. Weber and W. Thiel, *Theor. Chem. Acc.*, 2000, **103**, 495-506.
21. N. Otte, M. Scholten and W. Thiel, *J. Phys. Chem. A*, 2007, **111**, 5751-5755.
22. A. Koslowski, M. E. Beck and W. Thiel, *J. Comput. Chem.*, 2003, **24**, 714-726.
23. W. Domcke, D. R. Yarkony and H. Köppel, eds., *Conical Intersections: Electronic Structure, Dynamics and Spectroscopy*, World Scientific Publishing, Singapore, 2004.
24. T. Keal, A. Koslowski and W. Thiel, *Theor. Chem. Acc.*, 2007, **118**, 837-844.
25. J. C. Tully, *J. Chem. Phys.*, 1990, **93**, 1061-1071.
26. E. Fabiano, T. W. Keal and W. Thiel, *Chem. Phys.*, 2008, **349**, 334-347.
27. G. Granucci and M. Persico, *J. Chem. Phys.*, 2007, **126**, 134114.
28. E. Wigner, *Phys. Rev.*, 1932, **40**, 749-759.
29. N. Klaffki, O. Weingart, M. Garavelli and E. Spohr, *Phys. Chem. Chem. Phys.*, 2012, **14**, 14299-14305.
30. L. Verlet, *Phys. Rev.*, 1967, **159**, 98.
31. W. Thiel, *MNDO program*, version 6.1; Max-Planck-Institut für Kohlenforschung: Mülheim, 2007.
32. E. Fabiano, G. Groenhof and W. Thiel, *Chem. Phys.*, 2008, **351**, 111-116.
33. J. Contreras-García, E. R. Johnson, S. Keinan, R. Chaudret, J.-P. Piquemal, D. N. Beratan and W. Yang, *J. Chem. Theory Comput.*, 2011, **7**, 625-632.
34. E. R. Johnson, S. Keinan, P. Mori-Sánchez, J. Contreras-García, A. J. Cohen and W. Yang, *J. Am. Chem. Soc.*, 2010, **132**, 6498-6506.

35. R. F. W. Bader, *Chem. Rev.*, 1991, **91**, 893-928.
36. R. F. W. Bader, *Atoms in Molecules: A Quantum Theory.*, Oxford University Press, USA, 1991.
37. F. Weinhold and C. R. Landis, *Valency and Bonding. A Natural Bonding Orbital Donor-Acceptor Perspective*, Cambridge University Press, 2005.
38. J. P. Foster and F. Weinhold, *J. Am. Chem. Soc.*, 1980, **102**, 7211-7218.
39. E. L. Eliel and S. H. Wilen, eds., *Stereochemistry in Organic Compounds*, Wiley-Intersciencew, New York, 1994.
40. For the Z-isomer, the S_0 minimum is considered as there is no S_1 minimum.
41. M. Böckmann, N. L. Doltsinis and D. Marx, *Phys. Rev. E*, 2008, **78**, 036101.
42. M. Böckmann, N. L. Doltsinis and D. Marx, *J. Phys. Chem. A*, 2009, **114**, 745-754.
43. M. Böckmann, D. Marx, C. Peter, L. D. Site, K. Kremer and N. L. Doltsinis, *Phys. Chem. Chem. Phys.*, 2011, **13**, 7604-7621.
44. T. Cusati, G. Granucci and M. Persico, *J. Am. Chem. Soc.*, 2011, **133**, 5109-5123.